JOURNAL OF SPACECRAFT AND ROCKETS
Vol. 33, No. 2, March–April 1996

Ground Modal Tests of Space-Structure Components Using Boundary Masses

Mordechay Karpel* and Daniella Raveh†
Technion—Israel Institute of Technology, Haifa 32000, Israel
and
Sergio Ricci‡
Politecnico di Milano, 20133 Milan, Italy

A method for performing ground modal vibration tests of structural components, such that the resulting natural frequencies and vibration modes can be combined with those of neighboring components, is presented. The cost and technical difficulties associated with testing large and multiple-configuration structures can be greatly reduced with this approach. The method is based on testing the components with the interface coordinates loaded with rigid, heavy dummy masses supported by soft springs. With these boundary masses, the low-frequency modes contain local deformations near the interface and thus can be used to obtain accurate dynamic properties of the assembled structure. The method is demonstrated with measured natural frequencies and modes of a 19-m space-type truss, loaded at one end with a dummy mass. The measured data are used to predict the frequencies and modes of the original truss with free and clamped boundary conditions, and those of the double-length truss. The good agreement of the predicted results with test results on the unloaded structure and with analytical results on a tuned finite element model indicates that low-cost applications of the method to more complex structures are feasible.

Nomenclature

$\{F_b\}$	= vector of boundary forces
$[GM]$	= nominal generalized mass matrix, kg m^2
$[GM_f]$	= generalized mass matrix with fictitious masses, kg m^2
$[I]$	= unit mass matrix, kg m^2
$[K]$	= nominal stiffness matrix
$[K_f]$	= matrix of added boundary stiffness
$[\bar{K}_1]$	= coupled generalized stiffness matrix, N/m
$[M]$	= nominal mass matrix
$[M_f]$	= matrix of added boundary mass
$[\bar{M}_1]$	= coupled generalized mass matrix, kg m^2
$\{u\}$	= discrete displacement vector
$\{\xi\}$	= generalized displacements in Eq. (9)
$\{\xi_f\}$	= generalized displacements in Eq. (4)
$[\phi]$	= modes without fictitious masses
$[\phi_f]$	= modes with fictitious masses
$[\psi_n]$	= eigenvectors associated with Eq. (5)
$[\omega_f]$	= natural frequencies with fictitious masses, rad/s
$[\omega_n]$	= natural frequencies of the nominal component, rad/s

Subscripts

b	= boundary coordinates
i	= interior coordinates
1, 2	= group 1 or 2 in Eq. (11)
S	= symmetric boundary conditions
AS	= antisymmetric boundary conditions

Introduction

THE dynamic properties of elastic structures play an important role in the definition of structural design loads and in the design of stability and maneuver control systems. Structural dynamic effects may be of particular importance in space structures, where the almost null gravity, aerodynamic, and support loads allow low-weight, yet relatively large structures. Structures like those of large antennas and solar arrays require low weight and modular topology, for easy transportation and assembly, and high-performance control systems, for high-accuracy pointing requirements. The resulting structural and control systems are highly coupled, with the low structural natural frequencies well in the significant frequency range of the control system.

The dynamic properties used in the structural and control system designs are generally extracted from detailed finite element models. It is required to verify and correct these models by ground modal vibration tests, which provide sets of low natural frequencies, modal dampings, and mode shapes. The required laboratory size, the complex support system enabling the test article to carry its own weight, the very low elastic frequencies of the assembled structure, and the associated large deflections cause the full-scale ground tests to be extremely complicated, time-consuming, and expensive, and sometimes impossible. Special testing techniques, test facilities, instrumentation, and data reduction processes, needed to deal with these difficulties, are under development in several countries. The major relevant experimental facilities in the United States are described in Ref. 1. Some of the Japanese facilities are described in Ref. 2.

Research aimed at the development of low-cost techniques for vibration and active-control ground tests, sponsored by the Italian Space Agency (ASI), was started at the Politecnico di Milano in 1991.[3] The project, named Truss Experiment for Space Structures, started with the construction and testing of a 19-m space-type truss hanging on soft springs. The results of the first vibration tests, and their comparison with the finite element results, validated the instrumentation and the basic testing technique and provided data for further testing. Plans for changing the structure to a larger and more complex one are currently on hold because of lack of laboratory room and sufficient instrumentation.

The possibility of performing vibration tests of large structures by dividing them into substructures may offer a dramatic reduction of the test cost, the required laboratory room, and the required amount of instruments (shakers, sensors, support springs, and data acquisition systems). The main question is whether the individual component tests can provide sufficient dynamic information to adequately analyze the assembled structure. Techniques for performing numerical component mode synthesis for complex structures started in the sixties with formulations[4,5] based on the

Received Nov. 16, 1994; revision received May 12, 1995; accepted for publication May 15, 1995.

*Associate Professor, Faculty of Aerospace Engineering. Member AIAA.
†Graduate Student, Faculty of Aerospace Engineering.
‡Research Engineer, Department of Aerospace Engineering. Member AIAA.

assumption that the motion of each component, as part of the entire structure, is a linear combination of two sets of isolated component modes: 1) a number of low-frequency fixed-interface natural vibration modes and 2) all of the static constraint modes obtained by imposing a unit displacement on one of the interface coordinates while holding the remaining interface coordinates fixed. These modes contain detailed near-interface structural information, but the creation of fixed-interface conditions in actual tests might be impractical.

A different approach, where the component modes are calculated with free interface coordinates, was taken by Goldman[6] and by Hou.[7] These methods were more convenient because they used natural vibration modes only. However, with the interface points unloaded, vital information about the structural deformations near the interface is not included in the component modes, which leads to inaccuracies and slow convergence with the number of component modes. Benfield and Hruda[8] loaded the free interface coordinates with reduced stiffness and mass matrices of the neighboring substructures, and Hintz[9] and Rubin[10] added static attachment modes. These modifications, and those of hybrid coupling methods,[11] improved the results but, as in the fixed-boundary cases, are impractical for application in tests.

Karpel and Newman[12] based their modal synthesis approach on free component modes calculated with the interface coordinates loaded with large fictitious masses. The added large masses (which are cleaned in the coupling procedure) cause the low-frequency modal information to contain the necessary near-interface information without adding static constraint modes. Applications of the fictitious-mass method[12,13] demonstrated high accuracy and insensitivity to the magnitudes of the fictitious masses (provided they are large enough to cause significant local deformations). The simplicity and robustness of the fictitious-mass approach indicate its applicability in modal testing. Since the fictitious masses, when applied in test, are in fact real, we call them boundary masses instead. Limited applications of boundary masses in modal tests of Space Shuttle payloads have been reported.[14] The modes of the free payload connected to base masses were used for tuning a finite element model. The transformation from free-base to fixed-base modes was performed with the calculated finite element modes.

The main purposes of the work presented in this paper were to measure the modes of a space-type structure with boundary masses, to formulate the construction of modal-synthesis models that are based on the measured data, to apply this model to a variety of interface conditions, and to draw conclusions on the applicability of the boundary-mass method to testing large structures by parts.

Component with Fictitious Masses

The fictitious-mass modal synthesis method[12,13] is based on component modes calculated with large fictitious masses loading their boundaries. When applied in a ground vibration test, the boundary masses are limited in size and may have to be supported by springs. The free, undamped equation of motion of a structural component, loaded with boundary masses and springs, is

$$\begin{bmatrix} M_{ii} & M_{ib} \\ M_{ib}^T & M_{bb}+M_f \end{bmatrix} \begin{Bmatrix} \ddot{u}_i \\ \ddot{u}_b \end{Bmatrix} + \begin{bmatrix} K_{ii} & K_{ib} \\ K_{ib}^T & K_{bb}+K_f \end{bmatrix} \begin{Bmatrix} u_i \\ u_b \end{Bmatrix} = \{0\} \tag{1}$$

Equation (1) is solved for a set of fictitious natural frequencies (diagonal), modes, and generalized masses:

$$[GM_f] = [\phi_f]^T[M][\phi_f] + [\phi_{fb}]^T[M_f][\phi_{fb}] \tag{2}$$

where $[\phi_{fb}]$ includes the rows in $[\phi_f]$ associated with $\{u_b\}$.

The fictitious modes $[\phi_f]$ were used in Refs. 12 and 13 as the generalized coordinates of the component in the subsequent modal-synthesis cases. To gain more insight on the effects of the fictitious masses, the modes here are first transformed to those of the unloaded component (without the boundary masses and springs). The discrete-coordinate free undamped equation of motion of the unloaded component is

$$\begin{bmatrix} M_{ii} & M_{ib} \\ M_{ib}^T & M_{bb} \end{bmatrix} \begin{Bmatrix} \ddot{u}_i \\ \ddot{u}_b \end{Bmatrix} + \begin{bmatrix} K_{ii} & K_{ib} \\ K_{ib}^T & K_{bb} \end{bmatrix} \begin{Bmatrix} u_i \\ u_b \end{Bmatrix} = \{0\} \tag{3}$$

The basic assumption is that the n displacements in Eq. (3) can be expressed as a linear combination of n_f modes with boundary masses, $[\phi_f]$, where $n_f \ll n$, namely,

$$\begin{Bmatrix} u_i \\ u_b \end{Bmatrix} = \begin{bmatrix} \phi_{fi} \\ \phi_{fb} \end{bmatrix} \{\xi_f\} \tag{4}$$

Equations (2–4) yield the generalized-coordinate equation of motion of the nominal structure (of order n_f)

$$\left([GM_f] - [\phi_{fb}]^T[M_f][\phi_{fb}]\right)\{\ddot{\xi}_f\} + \left([\omega_f]^2[GM_f] - [\phi_{fb}]^T[K_f][\phi_{fb}]\right)\{\xi_f\} = \{0\} \tag{5}$$

Equation (5) can be solved for all the n_f natural frequencies $[\omega_n]$ and eigenvectors $[\psi_n]$. These natural frequencies are approximations of those of the unloaded component, Eq. (3). The associated natural vibration modes are approximated by

$$\begin{bmatrix} \phi_i \\ \phi_b \end{bmatrix} = \begin{bmatrix} \phi_{fi} \\ \phi_{fb} \end{bmatrix} [\psi_n] \tag{6}$$

and the generalized masses by

$$[GM] = [\psi_n]^T \left([GM_f] - [\phi_{fb}]^T[M_f][\phi_{fb}]\right)[\psi_n] \tag{7}$$

As will be demonstrated in the numerical application, the low frequencies in $[\omega_n]$ and the associated modes in $[\phi]$ are typically almost identical to those extracted from the unloaded finite element model. The high frequencies and modes reflect local deformations and are not necessarily actual natural modes.

Component as Part of a Larger Structure

The equation of motion of the component as part of free vibrations of the entire structure is Eq. (3) with boundary forces

$$\begin{bmatrix} M_{ii} & M_{ib} \\ M_{ib}^T & M_{bb} \end{bmatrix} \begin{Bmatrix} \ddot{u}_i \\ \ddot{u}_b \end{Bmatrix} + \begin{bmatrix} K_{ii} & K_{ib} \\ K_{ib}^T & K_{bb} \end{bmatrix} \begin{Bmatrix} u_i \\ u_b \end{Bmatrix} = \begin{Bmatrix} 0 \\ F_b \end{Bmatrix} \tag{8}$$

where $\{F_b\}$ is the vector of forces applied at the boundary by other components. We now express the displacements in Eq. (8) as a linear combination of the approximated unloaded modes, Eq. (6):

$$\begin{Bmatrix} u_i \\ u_b \end{Bmatrix} = \begin{bmatrix} \phi_i \\ \phi_b \end{bmatrix} \{\xi\} \tag{9}$$

In other words, as deduced from Eqs. (6) and (9), we transform our generalized displacements to $\{\xi\} = [\psi_n]\{\xi_f\}$. Since $[\psi_n]$ is a square nonsingular matrix, this transformation does not add errors beyond those introduced by the basic assumption of Eq. (4). Substitution in Eq. (8) and premultiplication by $[\phi_i^T \;\; \phi_b^T]$ yields

$$[GM]\{\ddot{\xi}\} + [\omega_n]^2[GM]\{\xi\} = [\phi_b]^T\{F_b\} \tag{10}$$

Application of Boundary Conditions

The modal coupling of several structural components is performed by imposing boundary displacement and force compatibility. The previous applications of the fictitious-mass method[12,13] assumed that in each connection of two components, one component is modeled as in Eq. (10), and the other one includes the interface coordinates as independent degrees of freedom. Reference 12 dealt with an arbitrary number of interface coordinates, and Ref. 13 simplified the formulation for statically determinate interconnections. The component interconnection in this paper is also assumed to be statically determinate, with $n_b = 6$ boundary coordinates in the

general case. To be able to interconnect components which have the same type of modal representation, we rephrase Eq. (9) as

$$\begin{Bmatrix} u_i \\ u_b \end{Bmatrix} = \begin{bmatrix} \phi_{i1} & \phi_{i2} \\ \phi_{b1} & \phi_{b2} \end{bmatrix} \begin{Bmatrix} \xi_1 \\ \xi_2 \end{Bmatrix} \tag{11}$$

where the n_b modes in group 1 are selected so that $[\phi_{b1}]$ is a square, nonsingular matrix. For free–free components, the six rigid-body modes are conveniently selected as the modes of group 1. In ground tests, the rigid-body modes become low-frequency modes of the almost undeformed structure on soft springs. Rearrangement of Eq. (11) yields

$$\begin{Bmatrix} u_i \\ u_b \end{Bmatrix} = \begin{bmatrix} \phi_{i1}\phi_{b1}^{-1} & \phi_{i2} - \phi_{i1}\phi_{b1}^{-1}\phi_{b2} \\ I & 0 \end{bmatrix} \begin{Bmatrix} u_b \\ \xi_2 \end{Bmatrix} \tag{12}$$

Substitution in Eq. (8), yields

$$\begin{bmatrix} \bar{M}_1 & -\bar{M}_1\phi_{b2} \\ -\phi_{b2}^T\bar{M}_1 & GM_2 + \phi_{b2}^T\bar{M}_1\phi_{b2} \end{bmatrix} \begin{Bmatrix} \ddot{u}_b \\ \ddot{\xi}_2 \end{Bmatrix} + \begin{bmatrix} \bar{K}_1 & -\bar{K}_1\phi_{b2} \\ -\phi_{b2}^T\bar{K}_1 & \omega_{n2}^2 GM_2 + \phi_{b2}^T\bar{K}_1\phi_{b2} \end{bmatrix} \begin{Bmatrix} u_b \\ \xi_2 \end{Bmatrix} = \begin{Bmatrix} F_b \\ 0 \end{Bmatrix} \tag{13}$$

where

$$[\bar{M}_1] = [\phi_{b1}]^{-T}[GM_1][\phi_{b1}]^{-1}$$

and

$$[\bar{K}_1] = [\phi_{b1}]^{-T}[\omega_{n1}]^2[GM_1][\phi_{b1}]^{-1}$$

where $[\omega_{n1}]$, $[\omega_{n2}]$, $[GM_1]$ and $[GM_2]$ are the block-diagonal partitions of $[\omega_n]$ and $[GM]$ associated with groups 1 and 2 of Eq. (11).

All of the cases in this paper are analyzed by applying a free or fixed condition to each boundary coordinate in Eq. (13). The free–free case can be analyzed by Eq. (13) with $\{F_b\} = 0$. It can be shown that the resulting eigenvalues are identical to those of Eq. (5). Clamped boundary conditions are obtained from Eq. (13) by imposing $\{u_b\} = 0$, which yields

$$\left[GM_2 + \phi_{b2}^T\bar{M}_1\phi_{b2}\right]\{\ddot{\xi}_2\} + \left[\omega_{n2}^2 GM_2 + \phi_{b2}^T\bar{K}_1\phi_{b2}\right]\{\xi_2\} = \{0\} \tag{14}$$

The natural frequencies of the double-length component, where the original component boundary coordinates define a plane of symmetry, are found by applying symmetric or antisymmetric boundary conditions. The boundary displacement and force vectors, $\{u_b\}$ and $\{F_b\}$ in Eq. (13) are divided into symmetric and antisymmetric ones. Symmetric modes are obtained with $\{u_{b\,AS}\} = 0$ and $\{F_{bS}\} = 0$. Hence, the elimination of the rows and columns associated with $\{u_{b\,AS}\}$ in Eq. (13) results in a homogeneous equation to be solved for the double-length symmetric natural frequencies and modes,

$$\begin{bmatrix} (\bar{M}_1)_S & -(\bar{M}_1\phi_{b2})_S \\ -\left(\phi_{b2}^T\bar{M}_1\right)_S & GM_2 + \phi_{b2}^T\bar{M}_1\phi_{b2} \end{bmatrix} \begin{Bmatrix} \ddot{u}_{bS} \\ \ddot{\xi}_2 \end{Bmatrix} + \begin{bmatrix} (\bar{K}_1)_S & -(\bar{K}_1\phi_{b2})_S \\ -\left(\phi_{b2}^T\bar{K}_1\right)_S & \omega_{n2}^2 GM_2 + \phi_{b2}^T\bar{K}_1\phi_{b2} \end{bmatrix} \begin{Bmatrix} u_{bS} \\ \xi_2 \end{Bmatrix} = \{0\} \tag{15}$$

Similarly, the antisymmetric frequencies and modes of the double-length component are obtained by setting $\{u_{bS}\} = 0$ and $\{F_{b\,AS}\} = 0$.

The eigenvectors in each one of the four boundary-condition cases are in terms of boundary and modal deflections, $\{u_b\}$ and $\{\xi_2\}$. The discrete-coordinate mode shapes are recovered from these eigenvectors by applying the transformation of Eq. (12).

Application to the Truss Model

The original test structure, before adding boundary masses, is a 54-bay beamlike truss suspended from the ceiling by three pairs of springs, as shown in Fig. 1. To keep the total cost low, the structure is built of commercial plastic display hardware, the Meroform M12 Construction System. Each bay is a repetitive 353-mm cubic module with one diagonal on each side, as shown in Fig. 2. The stiffness of each suspension spring is 104 N/m. The springs are 1.19 m long at rest and 2.4 m long with the truss attached. They are located at 15, 50, and 85% of the truss length. The diagonal tubes are assembled so that the horizontal (x–z) plane is a plane of symmetry. In this way, the natural lateral and axial vibration modes are structurally decoupled from the vertical and rotational ones. While the vertical–rotational rigid-body motion is against the suspension springs, the lateral–axial one is of a pendulum mechanism represented in the model by equivalent springs. Further details on the original truss and its modal tests are given in Ref. 3.

One end of the truss, at $X = 0$, is to be connected to other substructures at four points. MSC/NASTRAN finite element analysis, in which each point has six degrees of freedom, showed that the addition of rigid elements that interconnect these points has negligible effects on the 24 calculated natural frequencies and mode shapes in the frequency range of interest (0–26 Hz). Hence, it can be assumed that the boundary is statically determined. A dummy grid point was added to the model at the center of the boundary section (at $X = Y = Z = 0$) and was rigidly connected to the four connection points. The displacements and rotations of the added point are considered as the boundary displacements, $\{u_b\}$.

The structural model of the boundary mass is depicted in Fig. 3. The mass is 60 cm long, made of 3-cm-thick steel plates, and weights 113 kg (compared to the 81-kg truss). When connected to the truss,

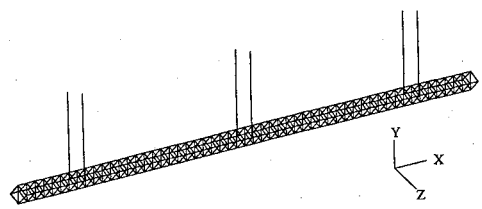

Fig. 1 Original truss.

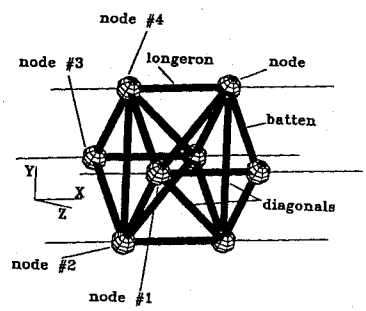

Fig. 2 Repetitive cubic module.

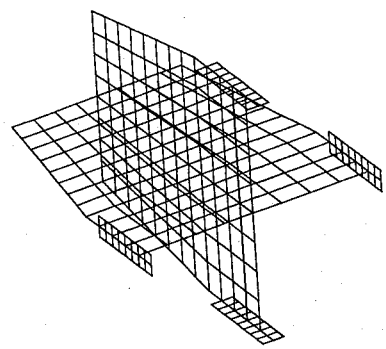

Fig. 3 Boundary mass.

the mass and moments of inertia of the boundary mass are large enough to cause significant truss deformations near the boundary in the low-frequency modes. Yet, its size and crosslike shape allow easy and safe handling, efficient excitation and vibration measurement, and convenient measurement of its inertial properties. The boundary mass is hanging on four similar, symmetrically positioned springs, each with stiffness of 220 N/m. While statically hung, the truss and the mass deflect in the same amount and remain horizontal. A separate finite element analysis of the boundary mass showed that its first natural frequency is 184 Hz, significantly higher than the frequency range of interest. The replacement of the detailed boundary-mass model by rigid elements had negligible effects on the 24 lowest natural frequencies of the mass-loaded truss. Consequently, all of the subsequent finite element analyses were performed with the rigid-body inertial properties of the boundary mass $[M_f]$ and the suspension stiffness terms $[K_f]$ attached to the dummy grid point at the center of the boundary section.

Modal Testing of the Mass-Loaded Truss

The decoupling between the lateral–axial modes and the vertical–rotational modes allowed the performance of two separate tests and subsequent analyses. The coupling between the vertical and the torsional motion makes the excitation, measurements, and mode identification in the vertical–rotational case more complicated. Hence, for the sake of simplicity and clarity, the test results and the subsequent analyses described in this paper are for the lateral–axial modes only. The vertical–rotational test and analysis gave similar results and lead to the same conclusions.

A picture of the mass-loaded truss during the modal tests is shown in Fig. 4. The tests were performed with the same equipment that was used for the free truss.[3] The issues that required special attention in the present tests were the relatively low frequencies because of the additional boundary mass and the requirement for high accuracy in measuring the modal deflections, especially at the boundary mass, to obtain accurate coupling results. Consequently, the test was performed in two steps. In the first step a band-limited white noise was used to excite the structure, just to roughly identify the natural frequencies. In the second step a stepped sine excitation was applied around the previously identified peaks, with a frequency resolution of 0.020 Hz, for accurate reconstruction of the mode shapes.

The excitation load was applied with a single APS long-stroke shaker positioned two bays from the boundary section. Accelerations were measured by eleven piezoelectric Structcel® accelerometers: three on the boundary mass (one in the x and two in the z direction) and eight on the truss (all in z). The response to each excitation was repeated with the eight truss accelerometers moved to other locations, which gave the modal displacements $[\phi_{fi}]$ at 16 interior truss points in the z direction. The three measurements on the boundary mass yielded the modal displacements $[\phi_{fb}]$ at the boundary point in the x, z, and θ_y directions. These coordinates represent the statically determined connection in the lateral–axial case.

The modal parameter identification was performed using the least-squares complex exponential technique, as implemented in the LMS software.[15] Out of the first 24 modes, 9 are lateral (2 pendulum and 7 elastic) and 2 are axial (1 pendulum and 1 elastic), with very small coupling between the axial and the lateral motion. The natural frequencies of the three pendulum modes are about 0.3 Hz. It was not possible to properly identify those modes below 0.7 Hz because of limitations in the instrumentation. The corresponding finite element modes were added instead to the set of measured flexible modes. The single elastic axial mode (10.91 Hz) was also taken from the finite element model. A comparison between the measured lateral elastic frequencies and those of the tuned finite element model is shown in Table 1. The mode numbers represent their sequence in the full model. The sum of the lateral squared errors was minimized by homogeneous fine tuning of the Young's modulus of all the short tubes.

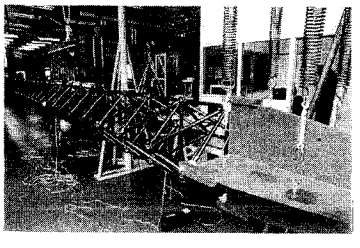

Fig. 4 Mass-loaded truss in modal testing.

Table 1 Lateral frequencies of the mass-loaded truss

Mode no.	F.E. freq., Hz	Test freq., Hz	Error, %
7	0.878	0.857	2.41
9	2.590	2.647	−2.16
11	5.070	5.249	−3.40
14	8.477	8.473	0.04
18	12.376	12.572	−1.55
20	16.945	16.885	0.36
23	21.534	21.528	0.03

Modal Coupling with the Measured Modes

The orthogonality of the measured modes was checked by calculating the supposedly diagonal generalized mass matrix $[GM_f]$ of Eq. (2) with the 11 measured modes (including the added rigid-body and axial ones), and with the mass matrix obtained by Guyan reduction[16] of the finite element matrix to the measured degrees of freedom. The orthogonality check showed some significant off-diagonal terms, especially in coupling between the rigid-body and the first bending mode. Observation of this mode showed that it contained significant lateral rigid-body motion, which is explained by the closeness of its natural frequency to the pendulum frequencies and to the instrumentation limit. Before being used in subsequent analyses, the measured modes were orthogonalized using the Gram–Schmidt procedure, starting with the pendulum modes. According to this procedure, the modes are changed sequentially when each modified mode is a linear combination of the original one and the previously orthogonalized modes, so that the modified $[GM_f]$ is a unit matrix.

Four coupling cases were analyzed, each case having different boundary conditions. The cases are free, clamped, double-length symmetric, and double-length antisymmetric truss. Case 1 (free) was analyzed by eigenvalue analysis of Eq. (5), case 2 (clamped) by Eq. (14), case 3 (symmetric) by Eq. (15) with $\{u_{bS}\}$ containing the boundary displacement in z only, and case 4 using the antisymmetric version of Eq. (15) with $\{u_{b\,AS}\}$ containing the boundary displacement in x and the rotation in θ_y. For each case the coupling analysis was performed twice: once using the 11 orthogonalized test modes, and once (for comparison) using the corresponding finite element modes.

Case 1 is the only one for which we can compare the coupling results with experimental measurements. Reference 3 describes the modal test of the unloaded truss. Fifteen frequencies were measured in the range of 0 to 10 Hz (including six rigid-body modes): only four of them correspond to lateral elastic modes (first to fourth bending). A comparison of these frequencies with the ones obtained by coupling of the 11 mass-loaded test modes is given in Table 2. It can be observed that the modal coupling yielded frequency errors of less than 5%. Considering the fact that large boundary masses were cleaned in the process based on measured boundary deflections, the comparison is very good.

The test-coupling frequencies, and the finite element coupling frequencies of case 1, are compared in Table 3 with the direct finite element frequencies of the free truss. This time the direct frequencies are considered the true ones. For most of the finite element coupling frequencies, except modes 19 and 23, the errors are extremely small, which agrees with previous computational applications of the fictitious-mass method. As expected, the errors are larger when the coupling is performed with test modes, but they are still under 5%. The large errors in mode 19, which is the only axial elastic mode, and in mode 23 are explained below.

The coupling mode shapes of case 1 were calculated by Eq. (6). Comparisons between the test coupling and the directly calculated mode shapes of case 1 are shown in Fig. 5. The plots are of the lateral deflections at the measurement points, connected by straight

Table 2 Free-boundary lateral frequencies (case 1): direct test vs coupling from test

Mode no.	Direct freq. from test, Hz	Coupling freq. from test, Hz	Error, %
7	1.16	1.168	0.69
10	3.21	3.273	1.97
11	6.04	6.315	4.55
14	9.83	9.888	0.59

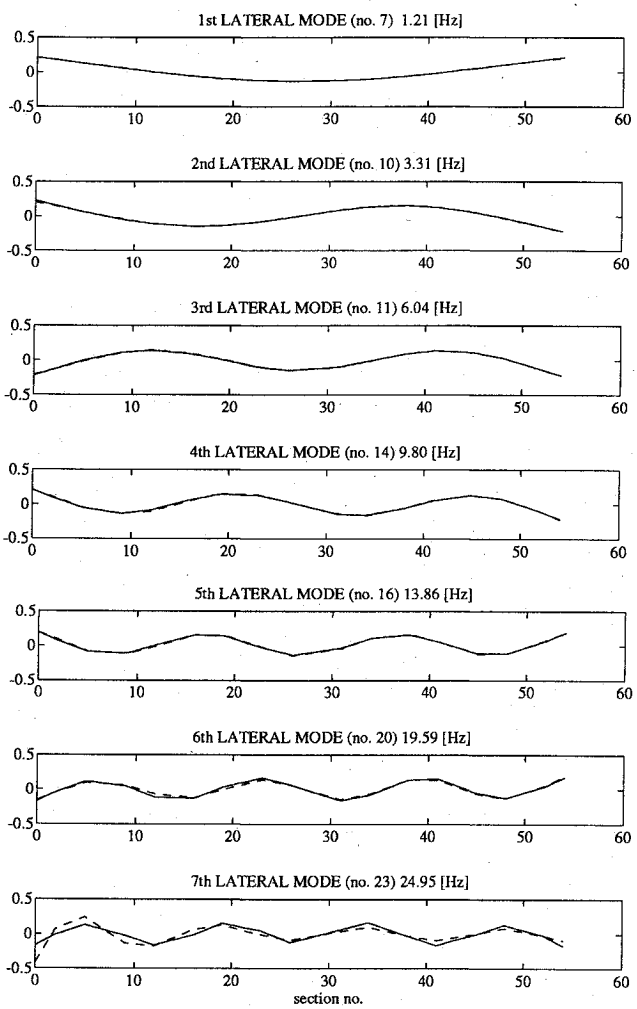

Fig. 5 Modes of the free unloaded truss–nominal vs test coupling modes: ——, NASTRAN and – – –, coupling.

lines. All the comparisons are excellent, except for that of the last mode, which shows large near-boundary bending distortions. These distortions, and the near-boundary axial distortions in mode 19 (not shown), are substantially different from those of the unloaded truss, in which they vanish near the boundary. This phenomenon explains the large frequency errors in modes 19 and 23 in Table 3. As explained previous to Eq. (10), these modes serve as generalized coordinates in cases 2 to 4. The local deformations in modes 19 and 23 are essential in these cases, where the boundary is not free.

The test coupling frequencies, and the finite element coupling frequencies of cases 2–4, are compared in Tables 4–6 with the respective direct finite element frequencies. Case 2 (Table 4) results in eight frequencies because the clamping constraints eliminate three degrees of freedom. The large errors of modes 19 and 23 in Table 3 do not appear in Table 4 because the clamped modes actually have large near-boundary distortions. On the other hand, the other errors in the case of coupling with finite element modes in Table 3 are generally smaller than the respective ones in Table 4. Larger boundary masses would reduce the clamped-boundary errors, but they might become difficult to handle in test.

Cases 3 and 4 are different combinations of the boundary conditions in cases 1 and 2. The symmetric case 3 (Table 5) resulted

Table 3 Free-boundary lateral frequencies (case 1): direct calculations vs coupling

No.	Direct f.e.	Coupling f.e.	Error, %	Coupling test	Error, %
1	0.301	0.300	−0.31	0.300	−0.31
2	0.301	0.301	−0.17	0.301	−0.17
3	0.303	0.303	−0.21	0.303	−0.21
7	1.211	1.212	0.04	1.168	−3.55
10	3.306	3.308	0.03	3.273	−1.01
11	6.037	6.040	0.04	6.315	4.59
14	9.802	9.808	0.06	9.888	0.88
16	13.855	13.873	0.13	14.389	3.85
19	17.645	19.280	9.27	19.303	9.40
20	19.593	19.868	1.40	19.875	1.44
23	24.955	35.052	0.46	35.646	42.84

Table 4 Clamped lateral frequencies (case 2): direct calculation vs coupling

No.	Direct f.e.	Coupling f.e.	Error, %	Coupling test	Error, %
1	0.355	0.356	0.34	0.356	0.43
3	1.201	1.216	1.28	1.204	0.25
6	3.300	3.352	1.58	3.295	−0.14
8	5.985	6.088	1.72	6.200	3.60
10	8.916	8.936	0.22	8.890	−0.29
11	9.737	9.912	1.80	10.024	2.95
14	13.767	14.004	1.71	14.363	4.33
16	19.462	19.837	1.93	19.918	2.34

Table 5 Symmetric lateral frequencies (case 3): direct calculations vs coupling

No.	Direct f.e.	Coupling f.e.	Error, %	Coupling test	Error, %
1	0.301	0.301	−0.17	0.301	−0.17
2	0.422	0.423	0.22	0.423	0.17
6	1.610	1.618	0.48	1.621	0.68
8	3.975	3.990	0.40	3.914	−1.53
10	7.012	7.038	0.37	7.081	0.99
13	8.923	8.944	0.23	8.926	0.03
14	10.961	10.992	0.28	11.045	0.77
16	15.179	15.218	0.26	15.521	2.25
19	20.706	20.741	0.17	20.793	0.41

Table 6 Antisymmetric lateral frequencies (case 3): direct calculations vs coupling

No.	Direct f.e.	Coupling f.e.	Error, %	Coupling test	Error, %
1	0.301	0.301	−0.17	0.301	−0.17
2	0.302	0.302	0.05	0.302	0.05
4	0.869	0.869	0.06	0.849	−2.28
6	2.657	2.658	0.04	2.708	1.94
9	5.238	5.241	0.05	5.449	4.02
11	8.859	8.872	0.14	8.922	0.71
14	12.974	13.013	0.30	13.363	3.00
16	17.642	18.743	6.23	18.766	6.37
17	18.541	19.437	4.83	19.418	4.73
20	23.801	28.861	21.26	29.033	21.98

in the smallest overall error level in both coupling cases. Only the first mode here is a rigid-body pendulum mode. Its frequency is very close to the first bending frequency (0.423 Hz), which would cause significant difficulties in an actual test with the double-length truss. The comparisons between the test coupling and the directly calculated symmetric mode shapes of case 3, shown in Figure 6, exhibit excellent agreement for all the modes. The test coupling modes were calculated here from the eigenvectors of Eq. (15) by the transformation of Eq. (12). The level of accuracy in the antisymmetric case 4 (Table 6), which is free in x and θ_y and restrained only in z, is similar to that of case 1.

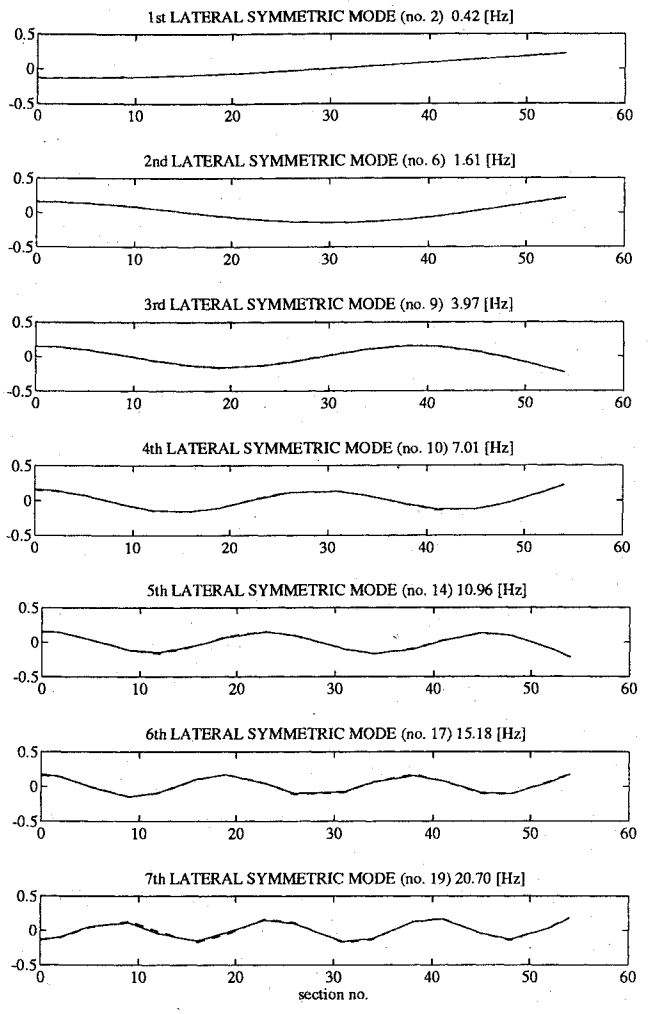

Fig. 6 Symmetric modes of the double-length truss–nominal vs test coupling modes: ——, NASTRAN and – – –, coupling.

Conclusions

The fictitious-mass modal coupling method was applied in this work, for the first time, with measured component modes. Ground vibration tests were performed for a space-type truss with one end attached to a relatively heavy, rigid, spring-supported boundary mass. Being based on one type of modes only, measured with no strict constraints at the boundary, the method was conveniently applied with standard methods of excitation, measurement, and data acquisition. The low sensitivity of the method to the size of the boundary-mass term allowed an easy design of the boundary mass with good handling and safety qualities. The mathematical formulation was reviewed and modified to allow adding the boundary springs, and to facilitate the application of different boundary conditions. Eleven lowest-frequency lateral–axial vibration modes were used to calculate the frequencies and modes of the unloaded truss with four different combinations of boundary conditions. Comparisons of the resulting lateral-bending frequencies with those obtained in a free-truss test showed differences of less than 5%. Similar accuracies were shown in the comparisons with direct finite element computations for all the analyzed cases, with excellent mode shape agreements, except for one or two high-frequency modes when some boundary coordinates were free. When based on computed modes, the coupling frequency errors were less than 2%. The good results indicate that measured component modes can be used for modal coupling with other components, which may eliminate the need for costly tests of large structures.

Acknowledgments

The work presented in this paper was partially supported by the ASI, under contract ASI 1991 RS 119, and by the Technion V.P.R. Fund–Albert Fund for Research and Development in Aerospace Engineering. The authors wish to thank D. Gallieni and R. Spairani for their cooperation in performing the test. Thanks are also extended to Amalia Ercoli-Finzi and Paolo Mantegazza for their continual advice and support.

References

[1]Sparks, D. W., Jr., and Juang, J. N., "Survey of Experimental Facilities for Control of Flexible Structures," *Journal of Guidance, Control and Dynamics*, Vol. 15, No. 4, 1992, pp. 801–816.

[2]Miura, K. "Adaptive Structures Research at ISAS, 1984–1990," *Journal of Intelligent Material Systems and Structures*, Vol. 13, No. 1, 1992, pp. 54–74.

[3]Bernelli Zazzera, F., Gallieni, D., and Ricci, S., "Modal Testing of a Large Space Structure Laboratory Model," *Proceedings of the 17th International Seminar on Modal Testing*, Katholike Univ., Lueven, Belgium, Vol. 2, 1992, pp. 1177–1185.

[4]Hurty, W. C., "Dynamic Analysis of Structural Systems by Component Modes," *AIAA Journal*, Vol. 3, No. 4, 1965, pp. 678–685.

[5]Craig, R. R., Jr., and Bampton, M. C. C., "Coupling of Substructures for Dynamic Analyses," *AIAA Journal*, Vol. 6, No. 7, 1968, pp. 1313–1319.

[6]Goldman, R. L., "Vibration Analysis by Dynamic Partitioning," *AIAA Journal*, Vol. 7, No. 6, 1969, pp. 1152–1154.

[7]Hou, S. N., "Review of Modal Synthesis Techniques and a New Approach," *Shock and Vibration Bulletin*, Vol. 40, Pt. 4, 1969, pp. 25–30.

[8]Benfield, W. A., and Hruda, R. F., "Vibration Analysis of Structures by Component Mode Substitution," *AIAA Journal*, Vol. 9, No. 7, 1971, pp. 1255–1261.

[9]Hintz, R. M., "Analytical Methods in Component Modal Synthesis," *AIAA Journal*, Vol. 13, No. 8, 1975, pp. 1007–1016.

[10]Rubin, S., "Improved Component-Mode Representation in Structural Dynamic Analysis," *AIAA Journal*, Vol. 13, No. 8, 1975 pp. 995–1006.

[11]Tran, D. M., "Hybrid Methods of Component Mode Synthesis," *Proceedings of the International Forum on Aeroelasticity and Structural Dynamics*, Vol. 2, AAAF, 1993, pp. 911–925.

[12]Karpel, M., and Newman, M., "Accelerated Convergence for Vibration Modes Using the Substructure Coupling Method and Fictitious Coupling Masses," *Israel Journal of Technology*, Vol. 13, 1975, pp. 55–62.

[13]Karpel, M., "Efficient Vibration Mode Analysis of Aircraft with Multiple External Store Configurations," *Journal of Aircraft*, Vol. 25, No. 8, 1988, pp. 747–751.

[14]Admire, J. R., Tinker, M. L., and Ivey, E. W, "Mass-Additive Modal Test Method for Verification of Constrained Structural Models," *AIAA Journal*, Vol. 31, No. 11, 1993, pp. 2148–2153.

[15]Anon., "LMS CADA-X Software," LMS International, Leuven, Belgium, 1990.

[16]Schaeffer, H. G., *MSC/NASTRAN Primer, Static and Normal Modes Analysis*, 3rd ed.,Wallace Press, Milford, NH, 1988.

E. A. Thornton
Associate Editor